

Numerical Instability Study of Supercritical Water Flowing Upward in Two Heated Parallel Channels

Sujuan Li, Vijay Chatoorgoon and Scott Ormiston

Abstract A three-dimensional (3D) numerical simulation has been carried out using a RANS model in CFD ANSYS CFX v15.0 to investigate the out of phase oscillation instability between two heated parallel channels with supercritical water flowing upward. Spatial and temporal grid sizes effects on flow instability are studied first. High sensitivity of the CFD code on time step size is investigated, while spatial grid size refinement influence is not noteworthy. Oscillatory instability boundaries of three experimental cases are predicated by CFD code with the standard $k-\varepsilon$ turbulence model. Chatoorgoon's 1D nonlinear SPORTS code is also used to determine the instability boundary for comparison purposes. These new numerical results are compared with experimental data and previous numerical results. In general, there is a good agreement between numerical instability results of this paper and the experiments. Certain instability thresholds difference is observed among different numerical simulations, and possible reasons are pointed out. A previous finding that CFD results clearly yield better predictions of the instability boundary than a 1D solution is disputed in this paper.

Keywords Supercritical water · Instability · Parallel channels · Numerical simulation · CFD

1 Introduction

In order to improve the economics and efficiency of the light water reactor (LWR) and make full use of the technologies of supercritical water-cooled fossil-fired power plants, a new concept reactor named supercritical water-cooled reactor (SCWR) was proposed as one of the most promising GEN-IV nuclear reactors. In Europe, a joint research project called high-performance light water reactor (HPLWR) has been formed for investigations of SCWR concept. In SCWR

S. Li · V. Chatoorgoon (✉) · S. Ormiston
University of Manitoba, Winnipeg, MB, Canada
e-mail: vijay.chatoorgoon@umanitoba.ca

loop design, water at 25 MPa and 500 °C leaves the reactor core, providing a high thermal efficiency of approximately 45% much higher than other LWRs (33%) [1]. Additionally, the direct cycle design of SCWR with coolant flowing from core to turbine directly at supercritical operating conditions makes installation of pressurizers, steam generators, recirculation pumps, and dryers unnecessary. This design simplification distinguishes a SCWR from other LWRs.

However, water properties will experience sharp changes as its temperature transitions through the pseudo-critical point, which can trigger thermal hydraulic instabilities. Flow instability in a nuclear reactor must be avoided as it is a mandatory safety requirement. As a result, the study of flow instability at supercritical pressure conditions has become popular, and large numbers of theoretical and numerical studies are emerging from around the world.

Zuber [2] theoretically investigated supercritical flow instability in a once through straight pipe flow system, and similar behaviors between supercritical flow instability and two-phase flow instability were found out. Chatoorgoon [3] performed an investigation about supercritical flow instability within natural circulation loop. Later he reported flow instability in heated parallel channels and derived a group of non-dimensional parameters which were validated by 94 numerical simulation cases [4]. Ambrosini and Sharabi [5] proposed two new dimensionless parameters for stability analysis of supercritical fluids. The newly derived non-dimensional parameters were a direct counterpart of the sub-cooling and phase change numbers introduced under two-phase flow conditions. Flow instability in single heated channel was simulated using the RELAP5 code and a 3D computational fluid dynamics (CFD) code by Ambrosini in 2007 [6], and the effects of inlet/outlet pressure loss coefficient and axial power distribution on stability boundary were reported. Xiong et al. [7, 8] performed both experimental and numerical studies on supercritical water flow instability in two heated parallel channels. Flow instability boundaries were obtained at different system pressures and inlet temperatures, and the experimental data were compared with their own 1D in-house code results, which proved that 1D numerical model can predict the onset of flow instability well. Subsequently, Xi et al. [9] also simulated Xiong's experiment with a 3D CFD code (an older version of CFX) and compared their results with experimental data. They concluded that their 3D model can predict the onset of instability better than Xiong's 1D model [8]. For the given geometry, a rather coarse mesh was used. Thus, their results and conclusion are revisited in this study. Xi et al. [10] also carried out another experimental investigation about flow instability between two heated parallel channels with supercritical water in 2014. The experimental loop was same as Xiong's [7], but Xi et al. used a much thicker wall channel in heated section and divided each heated channels into two sections to separately control the heating power. In this way, the influence of axial power shape on the flow instability was studied.

In this paper, both commercial CFD code ANSYS CFX v15.0 and Chatoorgoon's 1D nonlinear SPORTS code [11] were used to simulate Xiong's experiment [7]. For the CFD simulation, the standard $k-\varepsilon$ turbulence model with

scalable wall function was used. Obtained results were then compared with experiment and other previous numerical instability results.

2 Experimental Setup

A supercritical water loop had been constructed in Nuclear Power Institute of China, and more detailed information can refer to Xiong’s experiment paper [7]. Test section of this experimental loop is a two-parallel-channel system, and its schematic diagram is shown in Fig. 1. The two heated sections are INCONEL Alloy pipes with inner diameters 6 mm and heated length 3000 mm.

With these experimental facilities, a subsequent flow instability experiment had been carried out at different system pressures and inlet temperatures in 2012. Nine typical instability cases were obtained, summarized in Table 1. In this paper, cases: #1, 3, and 7 are simulated.

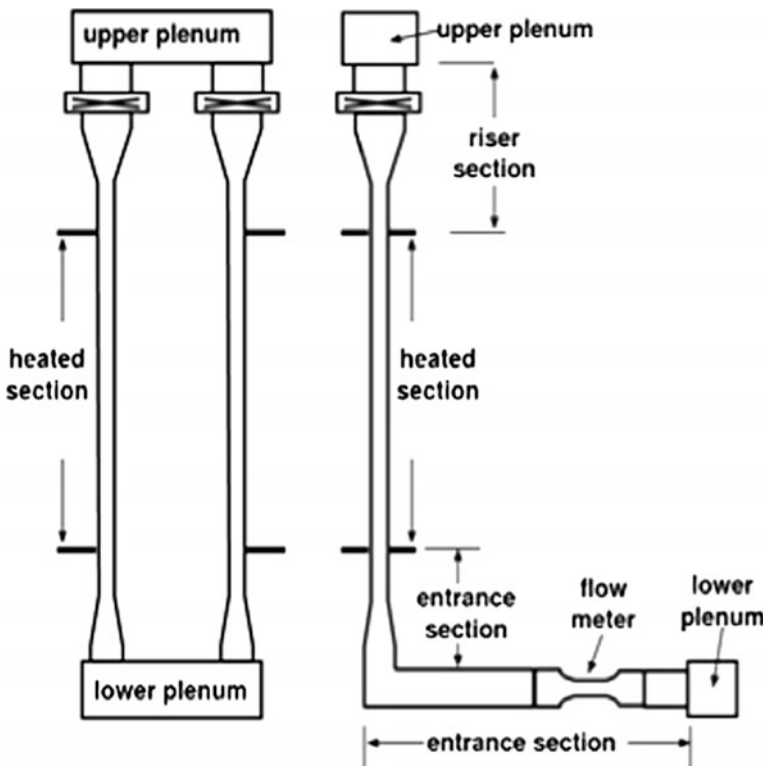


Fig. 1 Schematic of the experimental test section

Table 1 Experimental cases under different conditions

| Cases | System pressure (MPa) | Inlet temperature (K) | Inlet mass flow rate (kg/s) | Threshold power (KW) |
|--------|-----------------------|-----------------------|-----------------------------|----------------------|
| Case 1 | 23 | 453 | 0.0342 | 67.9 |
| Case 2 | 23 | 473 | 0.0333 | 66.0 |
| Case 3 | 23 | 493 | 0.0333 | 65.6 |
| Case 4 | 24 | 473 | 0.0333 | 67.0 |
| Case 5 | 24 | 493 | 0.0333 | 66.0 |
| Case 6 | 24 | 513 | 0.0331 | 64.6 |
| Case 7 | 25 | 473 | 0.0328 | 69.3 |
| Case 8 | 25 | 493 | 0.0333 | 68.9 |
| Case 9 | 25 | 513 | 0.0339 | 67.9 |

3 Numerical Modeling

3.1 Geometrical Model

The test section with two heated parallel channels is numerically modeled. Referring to Xiong's experiment [7] and 1D simulation paper [8], a simplified equivalent geometry was presented and that geometry was modeled here. The inner diameter of each heated channels was 6 mm. Plenum sizes were chosen large enough (length 430 mm, height 23 mm and width 10 mm) so that plenum effects on instability analysis are expectedly negligible.

Considering that the whole physical geometry is symmetrical, to save computational time only one half of the simplified model is simulated by applying a symmetry boundary condition. Figure 2a, b, respectively, illustrates the 3D view and specific dimensions of the geometrical model used in this study.

Due to manufacture and installation differences of the channels, asymmetry inlet and outlet pressure drop coefficients between the two parallel channels were previously reported by Xiong et al. [7]:

$$K_{in,1} = 5.40, K_{in,2} = 5.50, K_{out,1} = 4.93, K_{out,2} = 6.46$$

These K factors were also used in this study.

3.2 Governing Equations

The governing equations used in CFX are the standard mass, momentum, energy, and turbulence equations. Details of those equations can be found in [12].

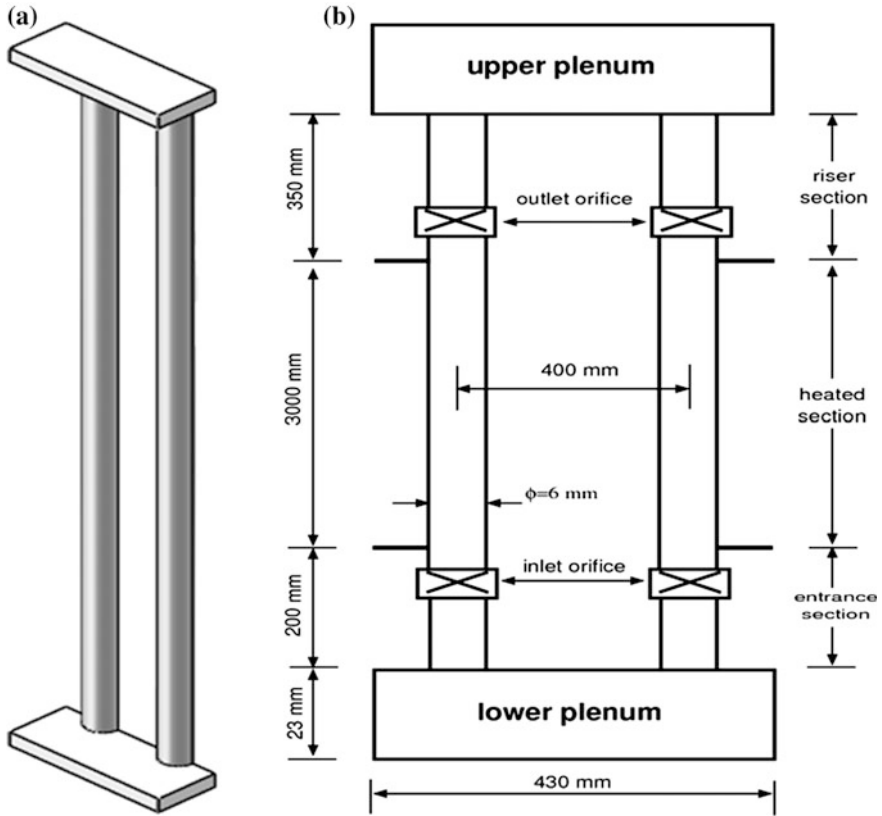


Fig. 2 a 3D view of simplified model. b Specific dimensions of simplified model

3.3 Domain Definitions and Boundary Conditions

To simulate local pressure drop with experimental K factors, subdomains are introduced. Domain separations are represented in Fig. 3, and Table 2 gives domain definitions as well as boundary conditions for each domain in Fig. 3.

3.4 Supercritical Water Properties

In CFX, thermodynamic properties of water stem from the IAPWS-IF97 database, formulated by Wagner et al. [13]. This database provides an accurate equation of state for water and steam properties. The range of validity for this property package in CFX is as follows:

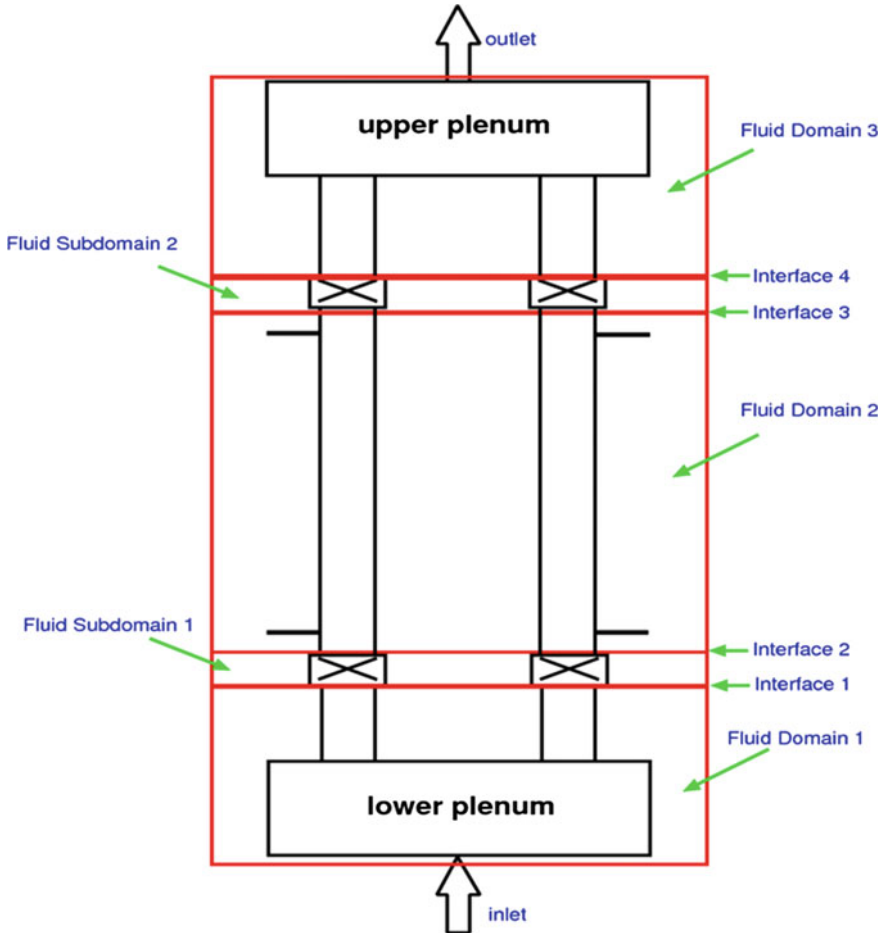


Fig. 3 Domain separations of simplified model

$$\begin{aligned}
 0(^{\circ}\text{C}) < T \leq 800(^{\circ}\text{C}) & \text{ for } 10(\text{MPa}) \leq P \leq 100(\text{MPa}) \\
 800(^{\circ}\text{C}) < T < 2000(^{\circ}\text{C}) & \text{ for } P < 10(\text{MPa})
 \end{aligned}$$

3.5 Numerical Solution Method

ANSYS CFX v.15.0 is used to generate meshes and solve the governing equations. The spatial domain is discretized into finite control volumes by CFX, and the governing equations are integrated over each control volume to ensure conservation of mass, momentum, energy, etc. Based on Rhie and Chow's work [14], a fully

Table 2 Domain definitions and boundary conditions

| | |
|------------------------|--|
| Fluid Domain 1, 2, & 3 | <ul style="list-style-type: none"> • Buoyancy model: $g_x = 0, g_y = -9.81 \text{ m/s}^2, g_z = 0, \rho_{\text{ref}} = 500 \text{ kg/m}^3$ • Turbulence model: standard $k-\epsilon$ with scalable wall function • Turbulent Prandtl Number: 0.95 • Buoyancy turbulence: production and dissipation |
| Fluid Subdomain 1& 2 | <ul style="list-style-type: none"> • General Momentum Source: $S_{M,x} = 0, S_{M,y} = -\frac{1}{2} \frac{K}{0.01} \frac{\dot{m}}{A} v, S_{M,z} = 0$ • Momentum source coefficient: $\frac{1}{2} \frac{K}{0.01} \frac{\dot{m}}{A}$ |
| Inlet | <ul style="list-style-type: none"> • Specified mass flow rate • Specified inlet temperature • Turbulence: medium intensity ($I = 5\%$) • Flow direction: normal to boundary condition |
| Outlet | <ul style="list-style-type: none"> • Relative pressure: 0 (Pa) |
| Wall | <ul style="list-style-type: none"> • No-slip wall with uniform heat flux for fluid domain 2 • No-slip adiabatic wall conditions for other domains |
| Symmetry | <ul style="list-style-type: none"> • Applied on the x-y plane that split geometry into half |
| Domain Interface | <ul style="list-style-type: none"> • Conservation of mass, momentum, turbulence, and heat transfer between two domains |

coupled solver that solves velocity and pressure equations as a single system is realized in CFX-5.

Double precision was used for the computations throughout. If the maximum normalized residual of each discretized equations was less than 1×10^{-6} , the steady state calculation was considered to be converged. For transient analyses, first-order transient scheme was used and the solver relaxation parameter was set to be 1.0 rather than the default value of 0.9. Furthermore, 30 iterations were performed during each time step. The high-resolution advection scheme was used for both steady state and transient analyses.

3.6 Numerical Procedure

3.6.1 Determining the Instability Threshold

Starting from a relatively high mass flow rate, a steady state analysis was done first to provide initial conditions for the corresponding transient runs. During the transient analyses, inlet and outlet channel mass flow rate responses with time were monitored to judge flow stability or instability.

For oscillatory instability, the flow would oscillate with diverging amplitudes in time. Converging flow oscillation amplitudes with time represented a stable system, while diverging amplitudes represented an unstable system. Theoretically,

instability threshold was defined as the mass flow rate that led to sustained mass flow rate oscillation without amplification or decay. When simulating particular experimental cases, a decrement of 0.0002 kg/s was applied to find the threshold mass flow rate. Within this change range, if the higher mass flow rate leads to stable flow while the lower mass flow rate triggers unstable flow, then the in-between mass flow rate was chosen as the threshold mass flow rate or instability boundary.

3.6.2 Spatial Grid Refinement Effects on Instability Boundary

Three meshes (see Table 3) with different spatial grid sizes were chosen to study grid refinement effects on instability boundary. For this study, 0.02 s was adopted as the time step size.

Oscillatory instability boundaries of case 1 and case 3 were predicted by CFD code with these three meshes, summarized in Table 4. If we choose the fine mesh (mesh 3) result as ‘best,’ the maximum difference in the threshold mass flow rate between mesh 1 and mesh 3 in case 3 is only 0.83%. Furthermore, considering the mass flow rate change used was 0.0002 kg/s (small enough), the instability boundaries predicted by these three different meshes are very close. Hence, spatial grid refinement does not make significant effects on the stability boundary. However, as a balance between reasonable results and convergence rate, mesh 2 with 450,000 nodes is considered adequate to be the final mesh for following analyses.

3.6.3 Time Step Size Effects on Instability Boundary

For case 1 in Table 1, the transient behavior of inlet mass flow rate in channel 1 at the four different time steps: 0.01, 0.02, 0.05, and 0.1 s were plotted and compared in Fig. 4.

Table 3 Meshes used for numerical simulation

| Meshes | Number of nodes |
|--------|-----------------|
| Mesh 1 | 150,000 |
| Mesh 2 | 450,000 |
| Mesh 3 | 1,000,000 |

Table 4 Instability boundaries predicted by CFD code with different meshes

| | Mesh 1 | Mesh 2 | Mesh 3 |
|--------|--------|--------|--------|
| Case 1 | 0.0341 | 0.0341 | 0.0343 |
| Case 3 | 0.0365 | 0.0360 | 0.0362 |

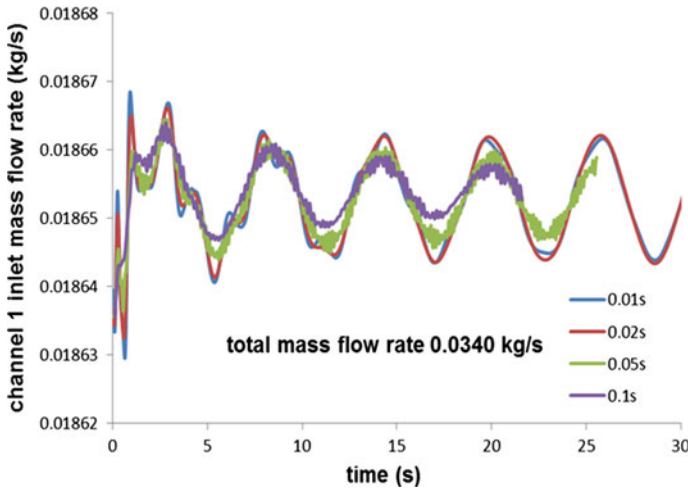


Fig. 4 Channel 1 inlet mass flow rate time response at different time steps

From Fig. 4, the effect of time step size on the transient mass flow rate can be discerned. With increasing the time step size from 0.01 s, the sine-wave oscillation shape becomes more rugged and less smooth, and its amplitude also decreases. Responses at 0.01 and 0.02 s collapse onto each other and agree reasonably well. The 0.05 and 0.1 s responses show that temporal convergence has not been achieved, and it would be wrong to use these time steps to determine the stability boundary. Furthermore, if we compare the threshold mass flow rates obtained with these four time steps (illustrated in Fig. 5), it can be noticed that 0.01 and 0.02 s predict essentially the same instability boundary. In addition, when the time step is increased from 0.02 to 0.1 s, the threshold mass flow rate drops strikingly from 0.0341 to 0.0321 kg/s, meaning the flow system becomes more stable with the larger time step. This is in agreement with the point of view proposed by Xiong et al. [8], obtained with their 1D code results.

To sum up the findings, 0.05 and 0.1 s are too large a time step for accurate stability analyses, and 0.02 s can be said to be the ‘optimum’ time step for it does not only require less computing efforts but also guarantee accuracy.

4 Results and Discussion

4.1 Prediction of Threshold Mass Flow Rate by CFD and 1D Codes

Three experimental cases (#1, 3, and 7) in Table 1 are numerically studied with a time step of 0.02 s and mesh 2.

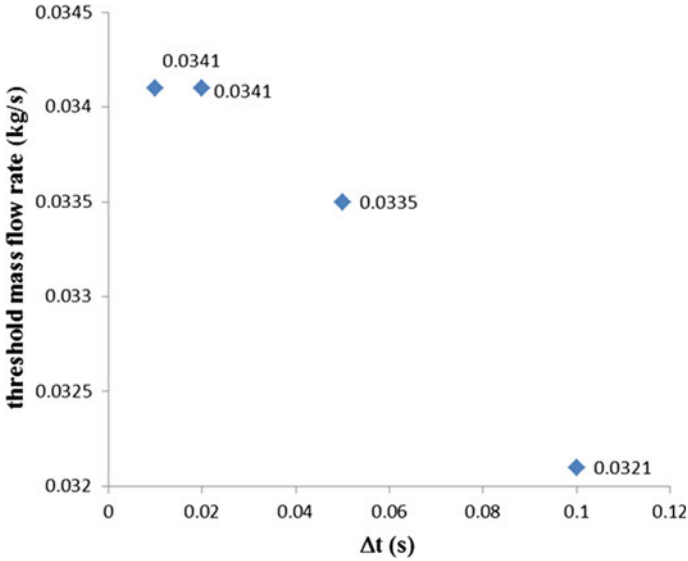


Fig. 5 Effect of time step on the threshold mass flow rate

Figure 6 indicates under case 1 flow conditions, the monitored inlet mass flow rate transient responses in channel 1 with total mass flow rate 0.0340 and 0.0342 kg/s. As shown in Fig. 6, for a total mass flow rate 0.0340 kg/s, the oscillation amplitude grows; contrarily, it decays for total mass flow rate 0.0342 kg/s. Therefore, the flow is unstable with a total mass flow rate of 0.0340 kg/s and is stable with a total mass flow rate of 0.0342 kg/s. Hence, 0.0341 kg/s is taken as the threshold mass flow rate of case 1.

The inlet boundary condition for this parallel channel system is constant total mass flow rate, so channel 1 and channel 2 will behave out of phase oscillation to conserve total mass flow rate, demonstrated in Fig. 7. Considering channel 2 has a larger outlet K factor, the mass flow rate in channel 2 is relatively smaller than that of channel 1.

Table 5 summarizes threshold mass flow rates predicted by 3D numerical CFD code for case 1, case 3, and case 7 in Table 1.

Oscillatory instability boundaries were also obtained by a 1D nonlinear SPORTS code [11] with the same flow conditions. Different from CFD code, calculating the wall shear friction automatically via the wall functions, a 1D code has to rely on an empirical friction-factor correlation to determine the friction pressure drop. Same as the 1D in-house code of Xiong et al. [8], Haaland approximate explicit relation [15] has been used for 1D SPORTS code.

Instability boundaries predicted by 1D nonlinear SPORTS code are listed in Table 6 below.

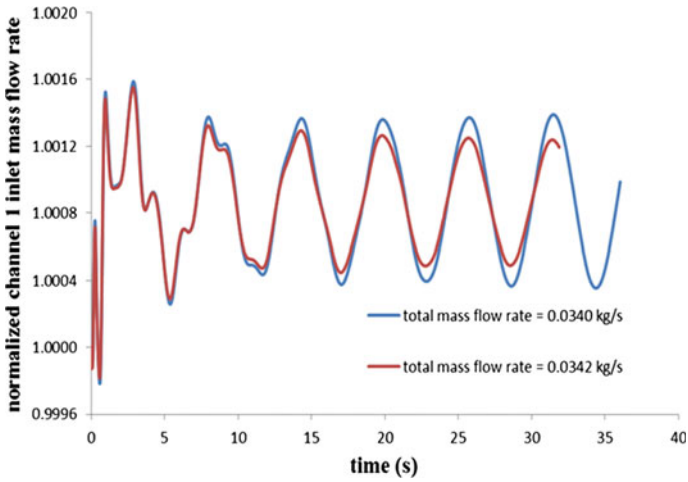


Fig. 6 Mass flow rate time responses with different mass flow rates for case 1

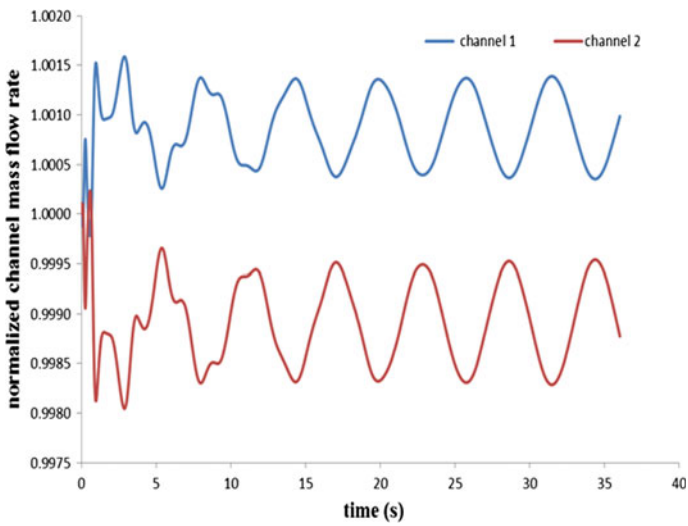


Fig. 7 Inlet mass flow rate responses with time in two parallel channels

Table 5 Threshold mass flow rates for different cases predicted by CFD code

| Cases | Threshold mass flow rate predicted by CFD (kg/s) |
|--------|--|
| Case 1 | 0.0341 |
| Case 3 | 0.0360 |
| Case 7 | 0.0349 |

Table 6 Threshold mass flow rates for different cases predicted by 1D non-linear code

| Cases | Threshold mass flow rate predicted by 1D nonlinear code (kg/s) |
|--------|--|
| Case 1 | 0.0338 |
| Case 3 | 0.0354 |
| Case 7 | 0.0346 |

4.2 Comparison Between Numerical Simulations and Experiment

For this flow instability experiment, about two heated parallel channels with supercritical water flowing upward, several numerical simulations (1D and 3D) have already been done and reported [8, 9]. In those studies, they held the flow rate constant and varied the total channel power until the threshold power was found. In this study, we held the power constant and varied the total mass flow rate until the stability boundary was found. We found that if the results are normalized to Ambrosini's dimensionless parameter [5], N_{TPC} , both approaches give exactly the same answer.

Figure 8 and Table 7 give the comparison of N_{TPC} between the calculated result and experimental result. Only three experimental cases (#1, 3, and 7) are presented in this paper due to time constraints. We plan to do additional simulations of other cases and will report on those cases later.

Considering the experimental uncertainty, which is expected to be at least $\pm 10\%$, the new numerical results presented here are considered to be within the experimental uncertainty.

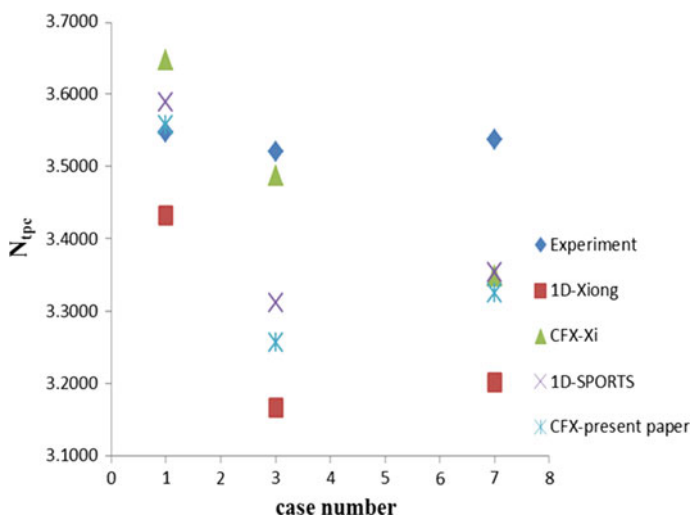
**Fig. 8** Comparison between the numerical simulation and experiment results

Table 7 N_{TPC} comparison between numerical simulation and experiment results

| Cases | Experiment [7] | 1D-Xiong [8] | | 1D-SPORTS [11] | | CFX-Xi [9] | | CFX-present paper | |
|--------|----------------|--------------|----------------|----------------|----------------|------------|----------------|-------------------|----------------|
| | | N_{TPC} | Relative Error | N_{TPC} | Relative Error | N_{TPC} | Relative Error | N_{TPC} | Relative Error |
| Case 1 | 3.5476 | 3.4326 | -3.24% | 3.5895 | 1.18% | 3.6468 | 2.80% | 3.5580 | 0.29% |
| Case 3 | 3.5200 | 3.1659 | -10.06% | 3.3112 | -5.93% | 3.4878 | -0.91% | 3.2560 | -7.50% |
| Case 7 | 3.5379 | 3.2010 | -9.52% | 3.3539 | -5.20% | 3.3490 | -5.34% | 3.3250 | -6.02% |

In general, there is no one group that predicts the best instability boundary compared with experiment. For example, CFX-present paper predicts best for case 1 with smallest relative error 0.29%; while for case 3, CFX-Xi gives the smallest relative error -0.91%. In spite of this, 1D code results carried out by Xiong et al. [8] deviate most from the experiment. We believe that was due to the pressure boundary condition they imposed at the inlet and outlet of the channels. They imposed equal static pressure at the channel inlet and outlet, whereas SPORTS imposes equal stagnation pressure at the channel inlet and outlet.

Firstly, if we compare the two 1D code results, 1D SPORTS code results are better in all cases. Reasons have already been mentioned above.

Secondly, if we compare the two 3D CFD code results, due to different CFX versions with different solver methods used, instability boundaries obtained are somewhat different. 3D numerical results obtained by Xi et al. [9] appear to be closer to the experiment, but our view is that their numerical results are not properly converged results due to the large time step used. Because of the 0.1-s time step, they will have a more stable flow system, leading to a higher N_{TPC} . Possibly, this is also one of the reasons why their N_{TPC} values of all three cases in Table 7 are higher than those of this paper.

Thirdly, if we compare 1D-SPORTS with 3D CFX-Xi results, except for case 3, 1D results of SPORTS code predict better than Xi’s 3D results. Therefore, the viewpoint proposed by Xi et al. [9] that 3D code would predict the onset of flow instability better than 1D code is not supported by these results.

Lastly, 1D-Xiong instability boundaries were also obtained with a time step of 0.02 s. If we only observe N_{TPC} distribution trend of 1D-Xiong, 1D-SPORTS and present CFX results in Fig. 8, we will notice that their trends are consistent, different from CFX-Xi’s trend with a 0.1-s time step. Hence, this interesting finding further proves the importance of time step size.

5 Conclusions

Both 3D and 1D numerical study are conducted to simulate flow instability between two parallel channels with supercritical water flowing upward. Present study results somewhat deviate from those reported by previous investigators. For 3D simulation differences, they may be related to dissipative and dispersive effects of large temporal and spatial grid size adopted in previous investigations. Different numerical

model and commercial code version used can also generate differences. 1D solution deviations of Xiong et al. are believed to be caused by imposing equal static pressure boundary condition at the channel inlet and outlet, whereas we believe it should be equal stagnation pressure.

Earlier finding that 3D code would predict the onset of flow instability better than 1D code is not supported by the results of this study. More experimental cases will be simulated to further compare 3D and 1D's capability to predict the instability boundary.

Spatial grid size refinement does not have a dramatic influence on the instability boundary, whereas there is a high sensitivity to the time step size.

References

1. Schulenberg, T., et al., Design and analysis of a thermal core for a high performance light water reactor. *Nuclear Engineering and Design*, 2011. 241(11): p. 4420–4426.
2. Zuber, N., An analysis of thermally induced flow oscillations in the near-critical and super-critical thermodynamic region: final report. 1966: Huntsville, AL: George C. Marshall Space Flight Center, 1966.
3. Chatoorgoon, V., Stability of supercritical fluid flow in a single-channel natural-convection loop. *International Journal of Heat and Mass Transfer*, 2001. 44(10): p. 1963–1972.
4. Chatoorgoon, V., A. Voodi, and D. Fraser, The stability boundary for supercritical flow in natural convection loops. *Nuclear Engineering and Design*, 2005. 235(24): p. 2570–2580.
5. Ambrosini, W. and M. Sharabi, Dimensionless parameters in stability analysis of heated channels with fluids at supercritical pressures. *Nuclear Engineering and Design*, 2008. 238(8): p. 1917–1929.
6. Ambrosini, W. and M.B. Sharabi, Assessment of stability maps for heated channels with supercritical fluids versus the predictions of a system code. *Nuclear Engineering and Technology*, 2007. 39(5): p. 627–636.
7. Xiong, T., et al., Experimental study on flow instability in parallel channels with supercritical water. *Annals of Nuclear Energy*, 2012. 48: p. 60–67.
8. Xiong, T., et al., Modeling and analysis of supercritical flow instability in parallel channels. *International Journal of Heat and Mass Transfer*, 2013. 57(2): p. 549–557.
9. Xi, X., et al., Numerical simulation of the flow instability between two heated parallel channels with supercritical water. *Annals of Nuclear Energy*, 2014. 64: p. 57–66.
10. Xi, X., et al., An experimental investigation of flow instability between two heated parallel channels with supercritical water. *Nuclear Engineering and Design*, 2014. 278(0): p. 171–181.
11. Chatoorgoon, V., SPORTS - A simple non-linear thermalhydraulic stability code. *Nuclear Engineering and Design*, 1986. 93(1): p. 51–67.
12. SAS IP, I. ANSYS CFX-Solver Theory Guide, Release 15.0. 2013.
13. Wagner, W., et al., The IAPWS Industrial Formulation 1997 for the Thermodynamic Properties of Water and Steam. *Journal of Engineering for Gas Turbines and Power*, 2000. 122(1): p. 150–184.
14. Rhie, C.M. and W.L. Chow, Numerical study of the turbulent flow past an airfoil with trailing edge separation. *AIAA Journal*, 1983. 21(11): p. 1525–1532.
15. Haaland, S.E., Simple and Explicit Formulas for the Friction Factor in Turbulent Pipe Flow. *Journal of Fluids Engineering*, 1983. 105(1): p. 89–90.